

ARTICLE

A New Viscoelastic Model for Polycarbonate Compressing Flow

Wei Cao^{1*} Yaqiang Shen² Shixun Zhang¹ Tao Wang³ Yakun Wu¹ Changyu Shen¹

1. National Engineering Research Center of Mold & Die, Zhengzhou University, Zhengzhou, Henan, 450002, China

2. Shenzhen Zhaowei Machinery & Electronics CO., LTD., Shenzhen, 518103, China

3. Beijing Institute of Aeronautical Materials, Beijing, 100095, China

ARTICLE INFO

Article history:

Received: 1 November 2018

Accepted: 9 November 2018

Published: 30 November 2018

Keywords:

Viscoelastic

Constitutive model

Compressing flow

Numerical simulation

ABSTRACT

To overcome the weakness of conventional models in describing compressing flow especially in start and end stages the shear rate derivative was added to the right side of the PTT constitutive equation. The ability of describing the well-known 'shear thinning' and 'stretch harden' phenomena was first illustrated by theoretical analysis. Then the governing equations for compressing flow were established in terms of incompressible and isothermal fluid, and the numerical method was constructed to discretize the equations and get the compressing flow solutions. In order to validate the model and numerical methods the experiments with four melt temperatures were conducted and the corresponding simulations were performed. The better agreements with experimental data indicates the modified PPT model is better than the original PTT model in prediction of compressing flow. In addition, the proposed model is also validated with low and high compressing speed experiments.

1. Introduction

Transparent polycarbonates (PC) have been widely used in optical engineering. In order to reduce the residual stresses which influence the optical properties, the injection/compression process is often applied in manufacturing transparent PC products. This process is divided into two successive stages: injection and compression. The rheological characteristics of polymer in injection period have been studied extensively by both experiments and simulations. The rheological behaviors in compression, however, have not received much attention

because the process has only been applied in recent years. Some softwares such as Moldflow usually applies the uniform rheological model, for example, Cross-WLF model^[1] to describe the rheological behaviors in the two different stages for convenience. But polycarbonate in compression has special characteristic which are different from injection as our previous work^[2] exhibited. It is necessary to characterize it with an appropriate model so as to control the manufacturing precisely. Therefore, a new viscoelastic model based on Phan-Thien-Tanner model^[3-4] for PC compression was constructed in this study.

*Corresponding Author:

National Engineering Research Center of Mold & Die, Zhengzhou University,
Zhengzhou, Henan, China;

E-mail: wcao@zzu.edu.cn.

Fund Project:

Financial supports from the National Science Foundation of China (No. 11672271, 11432003) The National Key Research and Development Program of China (No. 2016YFB0101602) for this research work are gratefully acknowledged.

Some researches have shown polymer melt exhibits viscoelasticity during compression^[5-9]. There are lots of viscoelastic models to describe the rheological behavior, such as Giesekus, Leonov, Oldroyd-B, extended Pom-Pom (XPP) and Phan-Thien–Tanner (PTT), but none of them has proven to be superior to others in describing all kinds of flow^[10]. Aboubacar et al. found the PTT model was better than the Oldroyd-B model in describing planar contraction flows with high Weissenberg number^[11]. Palmer and Phillips demonstrated PTT model was suitable to describe the flow combined shear and elongation characteristics^[12]. Furthermore, Cao and Kobayashi found that this model can well predict flow-induced stresses for non-equilibrium flow in injection molding^[13-14]. Thus the PTT model was used to as the base model for revision in this study.

Recently we found the compressing force varies as 'steep—steady —steep—steady' pattern, and none of current constitutive can describe the two steep increasing regions well^[2]. In addition we also found there was no significant difference between the popular viscoelastic models such as Leonov, PTT, XPP for compressing flow. It was found the shear rate changed rapidly in the two force unusual increasing regions through careful calculations. This drove us to account for the additional shear rate contribution by adding its derivative to the right side of the PTT constitutive equation just like the Oldroyd-B model did^[15]. The modified model combines both nonlinear viscoelastic characteristics of PTT and the capability of characterizing the rapid shear rate. Usually the reasonability of the proposed model requires to be demonstrated by theoretical analysis and experimental test. The nonlinear characteristic makes the analysis very difficult, but linearization and dimensionless methods can solve this problem efficiently especially for viscoelastic flow problem^[16-19]. The proposed model was first analyzed to be able to describe the well-known 'shear thinning' and 'stretch harden' phenomena. Then the numerical simulations and experiments were carried out to illustrate the validation. The comparisons were conducted with different melt temperatures and compressing speeds.

2. Modified PTT Model

In our previous work we found the compressing force exhibits abnormal increase in compression start and end stage due to irregular changes of shear rate, and neither viscous nor viscoelastic existing models can describe this phenomenon properly. Meanwhile it also showed the compressing flow exhibited nonlinear viscoelastic characteristics. Thus we revised the PTT model by adding the shear rate derivative term $\lambda' \overset{\nabla}{\mathbf{a}}$ at the right side of the

constitutive equation to account for the effects of rapid changes of shear rate $\dot{\gamma}$.

$$\left[1 + \frac{\lambda \epsilon}{\eta} tr(\boldsymbol{\tau})\right] \boldsymbol{\tau} + \lambda \overset{\nabla}{\boldsymbol{\tau}} = 2\eta \left(\dot{\boldsymbol{\gamma}} + \lambda' \overset{\nabla}{\dot{\boldsymbol{\gamma}}}\right) \tag{1}$$

here ϵ is the nonlinear parameter to eliminate the singularity in extensional viscosity, $tr(\boldsymbol{\tau})$ denotes the trace of the viscoelastic tensor $\boldsymbol{\tau}$, λ , η represent the relaxation time and viscosity coefficient respectively, and λ' is the parameter to control the effect of shear rate derivative. The upper convective derivative is defined as

$$\overset{\nabla}{\boldsymbol{\tau}} = \frac{\partial \boldsymbol{\tau}}{\partial t} + \mathbf{v} \cdot \nabla \boldsymbol{\tau} - \nabla \mathbf{v} \cdot \boldsymbol{\tau} - \boldsymbol{\tau} \cdot (\nabla \mathbf{v})^T \tag{2}$$

In order to verify the reasonability of the proposed model, we first illustrate whether it is capable to characterize the well-known phenomena of 'shear thinning' and 'stretch harden'.

2.1 Shear Thinning

For steady shear flow $u = \dot{\gamma}y, v = 0$ the constitutive equations are reduced to

$$\left(1 + \frac{\lambda \epsilon}{\eta} (\tau_{xx} + \tau_{yy})\right) \tau_{xx} - 2\lambda \dot{\gamma} \tau_{xy} = -2\eta \lambda' \dot{\gamma}^2 \tag{3}$$

$$\left(1 + \frac{\lambda \epsilon}{\eta} (\tau_{xx} + \tau_{yy})\right) \tau_{xy} - \lambda \dot{\gamma} \tau_{yy} = \eta \dot{\gamma} \tag{4}$$

$$\left(1 + \frac{\lambda \epsilon}{\eta} (\tau_{xx} + \tau_{yy})\right) \tau_{yy} = 0 \tag{5}$$

The nominal solution for this problem is

$$\left(1 + \frac{\lambda \epsilon}{\eta} \tau_{xx}\right)^2 \tau_{xx} + 2\left(1 + \frac{\lambda \epsilon}{\eta} \tau_{xx}\right) \lambda \eta \dot{\gamma}^2 - 2\lambda \eta \dot{\gamma}^2 = 0 \tag{6}$$

$$\tau_{xy} = \frac{\eta \dot{\gamma}}{1 + \frac{\lambda \epsilon}{\eta} \tau_{xx}} \tag{7}$$

$$\tau_{yy} = 0 \tag{8}$$

The Eq. (6) is a cubic equation about the stress component of τ_{xx} and can be solved with algebraic method, the solution is

$$\tau_{xx} = \frac{\eta}{\lambda \epsilon} \left[1 + (27\lambda - 9\lambda') \lambda \epsilon \dot{\gamma}^2 + 3\lambda \epsilon^{\frac{1}{2}} \dot{\gamma} \sqrt{6 + \left(-8 + 9\left(\frac{3\lambda}{\lambda'} - 1\right)^2\right) \lambda'^2 \epsilon \dot{\gamma}^2 + 24\lambda \lambda'^3 \epsilon^3 \dot{\gamma}^4} \right]^{\frac{1}{3}} \tag{9}$$

Then the stress component τ_{xy} can be determined

$$\tau_{xy} = \frac{\eta \dot{\gamma}}{1 + \left[1 + (27\lambda - 9\lambda') \lambda \epsilon \dot{\gamma}^2 + 3\lambda \epsilon^{\frac{1}{2}} \dot{\gamma} \sqrt{6 + \left(-8 + 9\left(\frac{3\lambda}{\lambda'} - 1\right)^2\right) \lambda'^2 \epsilon \dot{\gamma}^2 + 24\lambda \lambda'^3 \epsilon^3 \dot{\gamma}^4} \right]^{\frac{1}{3}}} \tag{10}$$

On using Eq. (10) the shear viscosity $\eta_{sh} (= \tau_{xy} / \dot{\gamma})$ is

calculated by

$$\eta_{ex} = \frac{\eta}{1 + \left[1 + (27\lambda - 9\lambda')\lambda\epsilon\dot{\gamma}^2 + 3\lambda\epsilon^{\frac{1}{2}}\dot{\gamma}\sqrt{6 + \left(-8 + 9\left(\frac{3\lambda}{\lambda'} - 1\right)\right)\lambda'^2\epsilon\dot{\gamma}^2 + 24\lambda\lambda'^3\epsilon^3\dot{\gamma}^4} \right]^{\frac{1}{3}}} \quad (11)$$

This formula means the viscosity decreases with increasing shear rate $\dot{\gamma}$, which indicates the model can describe 'shear thinning' effect.

2.2 Stretch Harden

For steady extension flow $u = \dot{\epsilon}x, v = -\frac{1}{2}\dot{\epsilon}y, w = -\frac{1}{2}\dot{\epsilon}z$, the modified PTT model is reduced to

$$\left(1 + \frac{\lambda\epsilon}{\eta}(\tau_{xx} + \tau_{yy} + \tau_{zz})\right)\tau_{xx} - 2\lambda\dot{\epsilon}\tau_{xx} = 2\eta\dot{\epsilon}(1 - 2\lambda'\dot{\epsilon}) \quad (12)$$

$$\left(1 + \frac{\lambda\epsilon}{\eta}(\tau_{xx} + \tau_{yy} + \tau_{zz})\right)\tau_{xy} - \frac{1}{2}\lambda\dot{\epsilon}\tau_{xy} = 0 \quad (13)$$

$$\left(1 + \frac{\lambda\epsilon}{\eta}(\tau_{xx} + \tau_{yy} + \tau_{zz})\right)\tau_{xz} - \frac{1}{2}\lambda\dot{\epsilon}\tau_{xz} = 0 \quad (14)$$

$$\left(1 + \frac{\lambda\epsilon}{\eta}(\tau_{xx} + \tau_{yy} + \tau_{zz})\right)\tau_{yy} + \lambda\dot{\epsilon}\tau_{yy} = -\eta\dot{\epsilon}(1 + \lambda'\dot{\epsilon}) \quad (15)$$

$$\left(1 + \frac{\lambda\epsilon}{\eta}(\tau_{xx} + \tau_{yy} + \tau_{zz})\right)\tau_{yz} + \lambda\dot{\epsilon}\tau_{yz} = 0 \quad (16)$$

$$\left(1 + \frac{\lambda\epsilon}{\eta}(\tau_{xx} + \tau_{yy} + \tau_{zz})\right)\tau_{zz} + \lambda\dot{\epsilon}\tau_{zz} = -\eta\dot{\epsilon}(1 + \lambda'\dot{\epsilon}) \quad (17)$$

Eqs. (13) - (14) indicate . Substituting this formula to Eq. (12) and Eqs. (15) - (16) yields

$$\tau_{xx} = -\frac{4\eta(1 - 2\lambda'\dot{\epsilon})}{3\lambda} \quad (18)$$

$$\tau_{yy} = -\frac{2\eta(1 + \lambda'\dot{\epsilon})}{3\lambda} \quad (19)$$

$$\tau_{zz} = -\frac{2\eta(1 + \lambda'\dot{\epsilon})}{3\lambda} \quad (20)$$

$$\tau_{yz} = 0 \quad (21)$$

The extension viscosity can be determined

$$\eta_{ex} = \frac{\tau_{xx}}{\dot{\epsilon}} = \frac{4\eta}{3\lambda} \left(2\lambda' - \frac{1}{\dot{\epsilon}}\right) \quad (22)$$

This formula indicates the extension viscosity increases as the extension rate $\dot{\epsilon}$ increases, which means the model can describe 'stretch harden' behavior.

3. Compressing Flow Simulation

In this study, the fully filled PC fluid was compressed at a constant velocity (\dot{h}) and flow out at disc brims, shown as Fig. 1. The melt flow was limited within the geometric region: $0 \leq r \leq R$ and $0 \leq z \leq h(t)$. The compressing flow was, due to the changing height $h(t)$, inherently transient and inhomogeneous flows.

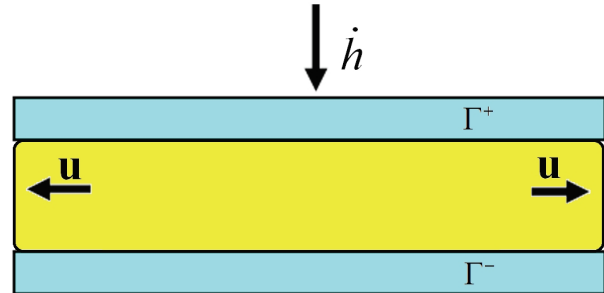


Figure 1. Schematic illustration of fully compressing flow.

3.1 Governing Equations

Compared with viscous force the gravitational and inertial forces are small and ignored. The governing equations for isothermal, incompressible and viscoelastic flow in cylindrical coordinates can be written

$$\frac{1}{r} \frac{\partial}{\partial r}(rv_r) + \frac{\partial}{\partial z}v_z = 0 \quad (23)$$

$$-\frac{\partial p}{\partial r} + \frac{1}{r} \frac{\partial}{\partial r}(r\tau_{rr}) + \frac{\partial}{\partial z}\tau_{rz} = 0 \quad (24)$$

$$-\frac{\partial p}{\partial z} + \frac{1}{r} \frac{\partial}{\partial r}(r\tau_{rz}) + \frac{\partial}{\partial z}\tau_{zz} = 0 \quad (25)$$

here r and z are the radial and axial coordinates respectively, v_r and v_z are the corresponding velocity components, p is the pressure, and τ_{rr} , τ_{rz} and τ_{zz} are the stress components.

During compression the container keeps open at the edges, therefore the pressure at the disc rim can be assumed zero.

$$p = 0 \text{ at } r = R \quad (26)$$

No slip boundary conditions for radial velocity were used on both top and bottom discs.

$$v_r = 0, v_z = 0 \text{ at } z = 0 \text{ } (\Gamma^-) \quad (27)$$

$$v_r = 0, v_z = \dot{h} \text{ at } z = h \text{ } (\Gamma^+) \quad (28)$$

In this study, the compressing velocity of the upper disc keeps constant, i.e. $v_z = \dot{h} = \frac{dH}{dt} = const$. Thus all the axial ve-

locity v_z at the same level is equal, which means $\frac{\partial v_z}{\partial r} = 0$.

3.2 Stresses

The stress tensor in viscoelastic fluid can be expressed as a sum of Newtonian and viscoelastic components:

$$\sigma = \tau_s + \tau_v \tag{29}$$

here τ_v is the extra stress tensor due to viscoelasticity and τ_s is the stress component of a Newtonian fluid given by

$$\tau_s = 2\eta_s \dot{\gamma} \tag{30}$$

The viscoelastic stress tensor is the sum of different modes

$$\tau_v = \sum_i \tau_i \tag{31}$$

The *i*th mode stress τ_i is governed by modified PTT model

$$\left[1 + \frac{\lambda_i \epsilon}{\eta_i} tr(\tau_i) \right] \tau_i + \lambda_i \overset{\nabla}{\tau}_i = 2\eta_i \left(\dot{\gamma} + \lambda_i \overset{\nabla}{\dot{\gamma}} \right) \tag{32}$$

here λ_i , η_i are the relaxation time and viscosity coefficient of *i*th mode.

3.3 Numerical Method

The momentum equations (24)–(25) subject to stress expression can be written as

$$-\frac{\partial p}{\partial r} + 2\eta_s \frac{\partial^2 v_r}{\partial r^2} + \eta_s \frac{\partial^2 v_r}{\partial z^2} + \sum_{i=1}^M \left(\frac{\partial \tau_{i,rr}}{\partial r} + \frac{\partial \tau_{i,rz}}{\partial z} \right) = 0 \tag{33}$$

$$-\frac{\partial p}{\partial z} + \eta_s \frac{\partial^2 v_r}{\partial r \partial z} + 2\eta_s \frac{\partial^2 v_z}{\partial z^2} + \sum_{i=1}^M \left(\frac{\partial \tau_{i,rz}}{\partial r} + \frac{\partial \tau_{i,zz}}{\partial z} \right) = 0 \tag{34}$$

Due to the coupled relationship between velocity, pressure and stress in governing equations and constitutive equations and the nonlinearity the analytical solutions for compressing flow can hardly be obtained even for a simple flow. The numerical methods have to be used to determine the discrete solutions. In this study, the finite difference method (FDM) was employed to determine the numerical solution because the PC flow was limited within a cylindrical rectangular region $0 \leq r \leq R; h \leq z \leq H$, which is suitable for FDM calculation. To keep the numerical consistence and stability, the forward difference and central difference schemes were used to discretize the one order and two order differential terms respectively, and the 'up-wind' scheme was used to discretize the convective term in constitutive equations. The differential equations corresponding to mass conservative equation (23), momentum equations (33)-(34) and constitutive equation (32) were discretized as

$$\frac{1}{r_i} \frac{v_{r,ij}^n - v_{r,i-1j}^n}{\Delta r} + v_{r,i}^n + \frac{v_{z,ij}^n - v_{z,ij-1}^n}{\Delta z} = 0 \tag{35}$$

$$-\frac{p_{ij}^n - p_{i-1j}^n}{\Delta r} + 2\eta_s \frac{v_{r,i-1j}^n - 2v_{r,ij}^n + v_{r,i+1j}^n}{\Delta r^2} + \eta_s \frac{v_{r,ij-1}^n - 2v_{r,ij}^n + v_{r,ij+1}^n}{\Delta z^2} + \sum_k \left(\frac{\tau_{k,rr,ij}^n - \tau_{k,rr,i-1j}^n}{\Delta r} + \frac{\tau_{k,rr,ij}^n - \tau_{k,rz,ij-1}^n}{\Delta z} \right) = 0 \tag{36}$$

$$-\frac{p_{ij}^n - p_{ij-1}^n}{\Delta z} + \eta_s \frac{v_{r,i+1j+1}^n + v_{r,i-1j-1}^n - v_{r,i-1j+1}^n - v_{r,i+1j-1}^n}{\Delta r \Delta z} + 2\eta_s \frac{v_{z,ij-1}^n - 2v_{z,ij}^n + v_{z,ij+1}^n}{\Delta z^2} + \sum_k \left(\frac{\tau_{k,rz,ij}^n - \tau_{k,rz,i-1j}^n}{\Delta r} + \frac{\tau_{k,zz,ij}^n - \tau_{k,zz,ij-1}^n}{\Delta z} \right) = 0 \tag{37}$$

$$\left[1 + \frac{\lambda_k \epsilon}{\eta_k} tr(\tau_k^n) \right] \tau_k^n + \lambda_k \frac{\tau_k^{n-n-1}}{\Delta t} + \mathbf{v}_{ij}^{n-1} \cdot \left(\frac{(\tau_{k,ij}^n - \tau_{k,i-1j}^n)/\Delta r}{(\tau_{k,ij}^n - \tau_{k,ij-1}^n)/\Delta z} \right) - \left(\frac{(\mathbf{v}_{ij}^n - \mathbf{v}_{i-1j}^n)}{\Delta r} \cdot \frac{(\mathbf{v}_{ij}^n - \mathbf{v}_{i-1j}^n)}{\Delta z} \right) \cdot \tau_k^n - \left(\frac{(\mathbf{v}_{ij}^n - \mathbf{v}_{i-1j}^n)}{\Delta r} \right) \cdot \left(\frac{(\mathbf{v}_{ij}^n - \mathbf{v}_{i-1j}^n)}{\Delta z} \right) = 2\eta_k \left(\dot{\gamma} + \lambda_i \overset{\nabla}{\dot{\gamma}} \right) \tag{38}$$

As the stress trace $tr(\tau_k^n)$ was also unknown, the above algebraic equations are nonlinear and the Newton-Raphson iterative method was employed to determine the solutions.

When all the solutions for discrete nodes were determined, the vertical force at every node of upper disc was calculated with the following formula

$$F_{jk} = \left[p_{jk} + \sum_{i=1}^M (\tau_{i,rz} + \tau_{i,zz})_{jk} \right] \tag{39}$$

Then integrate the discrete force F_{jk} with bilinear interpolation scheme to get the compressing force imposed on the upper disc.

$$F_{comp} = \iint_{A_{jk}} F_{jk}(r, z) dA \tag{40}$$

4. Results and Discussion

4.1 Experiments Set Up

ARES G2 rheometer (TA Instruments) was used to examine the melt rheological behavior during compressing. It cannot measure the viscosity or modulus in the process directly, but the compression force which closely relates the melt stress can be measured if the configuration is properly set up. On the other hand, this force can be calculated with formula (40) through discretization of the constitutive model and governing equations. Compare

Table 1. Measured relaxation times and moduli of 5 melt temperatures with ARES G2.

270°C		280°C		290°C		300°C		310°C	
Relaxation time λ_i (s)	Modulus G_i (Pa)	Relaxation time λ_i (s)	Modulus G_i (Pa)	Relaxation time λ_i (s)	Modulus G_i (Pa)	Relaxation time λ_i (s)	Modulus G_i (Pa)	Relaxation time λ_i (s)	Modulus G_i (Pa)
5.02923	76.5606	4.73195	51.3094	4.15657	46.913	3.0891	40.0322	2.0203	35.5218
0.583092	70.8121	0.22218	108.292	0.41924	50.135	0.363904	42.1809	0.31873	35.7013
5.56E-03	81150	9.52E-3	17602.6	5.59E-03	20158.2	8.97E-3	2983.95	3.57E-3	1867.95
8.56E-04	494619	9.05E-4	398497	6.77E-04	381588	5.83E-4	218261	4.63E-4	174874

Table 2. Simulated precisions of the two models for the four temperatures at compressing speed 0.01 mm/s

Temperature (°C)	PTT				Modified PTT			
	Difference			Variance	Difference			Variance
	Average	Start	End		Average	Start	End	
270	0.144836	0.464944	0.21165	0.014601	0.030326	0.025992	0.135206	0.003148
280	0.110653	0.144768	0.14169	0.004173	0.030326	0.075748	0.044342	0.000564
290	0.040754	0.13687	0.04062	0.00122	0.020929	0.035929	0.021636	0.000213
300	0.043427	0.022662	0.11008	0.001444	0.02439	0.013815	0.019223	0.000222

the differences between measured and simulated data can evaluate the correctness and advantages of the constitutive model.

The specimen was a thin disc with a diameter of 25 mm, and the compression started from 1.43 mm and stopped at 1.0 mm. To avoid polymer melt absorbing moisture in the air, the nitrogen was sweeping the disc during experiments. The rectangle of $r \times h$ in a cylindrical coordinate system was discretized to 100×20 small rectangles for FDM simulation.

The experimental material was polycarbonate, OQ 2720, Saibic Inc. The rotating rheological experiments were first carried out at melt temperatures of 270 °C, 280 °C, 290 °C and 300 °C to get the corresponding relaxation times and moduli listed in Tab. 1. Then the compressing experiments were performed at the four temperatures with compressing speed 0.01 mm/s. These experimental data were used to fit modified model and get the most appropriate constants $\lambda' = 0.561$ and $\epsilon = 0.425$. To validate the proposed model, the additional experiments were conducted with compressing velocities of 0.005mm/s and 0.02mm/s at 300 °C.

4.2 Melt Temperature Effects

Fig. 2 shows the compressing forces vary in the same trend for different melt temperatures, i.e. rapid increase at the onset, steady growth in the middle stage and rapid increase again at the end. Both PTT and modified PTT models can correctly predict this tendency but the simulated precisions have significant differences, see Tab. 2. The average simulated precisions have been improved 2~3 times

by modifying PTT. The remarkable differences happen in the compression start and end stages which shear rate varies violently, for example, the simulated difference of modified PTT for 270 °C is 0.025992 at start compressing stage, this value of the original PTT rises to 0.464944, almost twenty times of the modified model. In addition, the average simulated variances for PTT model are 4~8 times of the modified model for the four melt temperatures. Both Fig.2 and Tab. 2 indicate the modified PTT model better describes the rheological behavior than the original PTT model.

At the beginning of compression, the compressing force does not transfer to the bottom plate instantly and only the melt near the upper disc begins to flow, so the shear rates of the moving layers changes rapidly during this period. When all the melt within in the two discs flows to the brim the shear rate changes little, which do not cause much stress variation, and the compressing force increase steadily in the middle stage. Due to the gap is remarkable reduced in the end stage, the shear rate changes sharply again. For example, the decrease rate and increase rate of shear rate for 290 °C melt temperature reach 0.01658 and 0.00137 at the start and end stages respectively, which are considerable larger than the increase rate of 0.00041 in the middle stage, see Fig. 3. The violent changes of shear rate can influence the shear stresses and the close related compressing forces subsequently. Due to the contribution of shear rate change $\dot{\gamma}$ was accounted, the modified PTT model significantly improved the simulating precisions especially at the start and end stages.

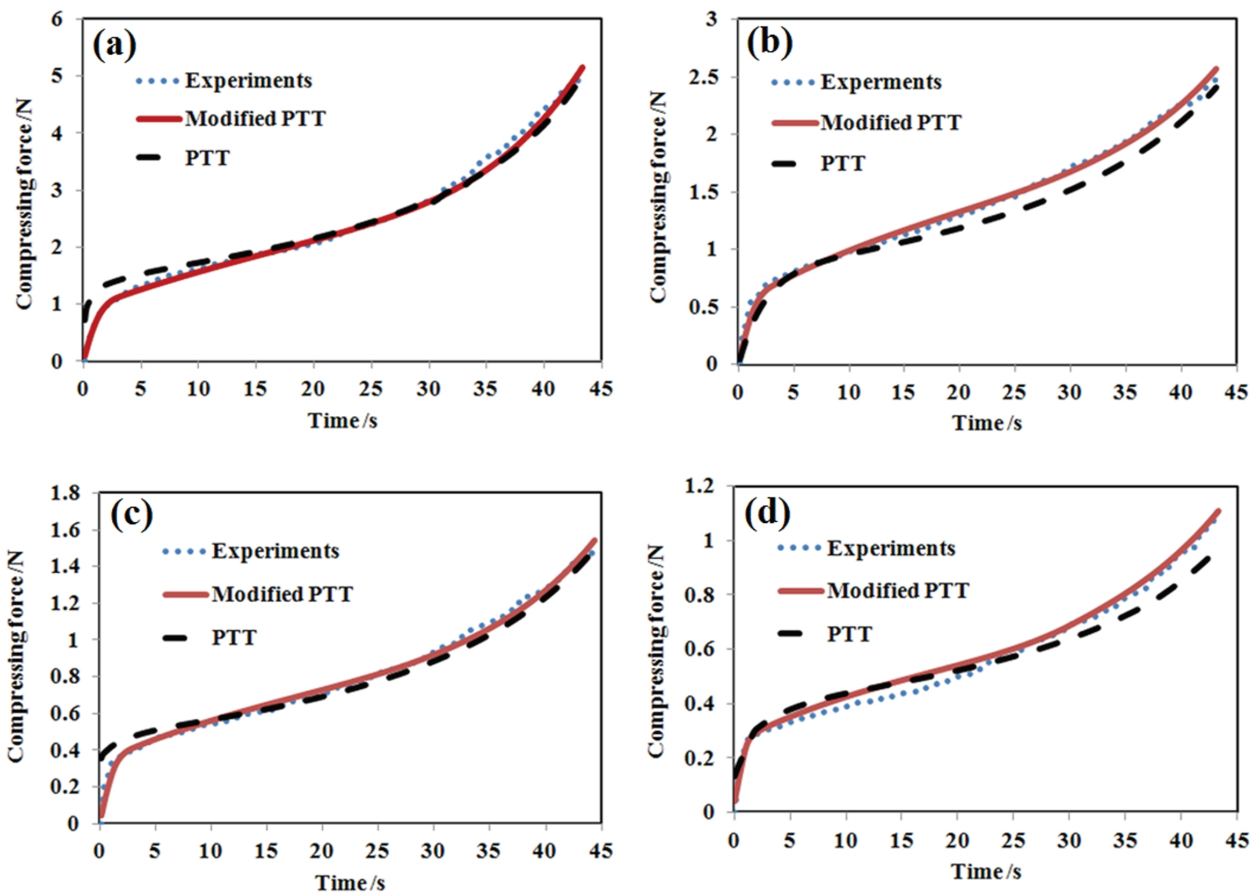


Figure 2. Compressing force varies with time for PC at compressing speed 0.01 mm/s with melt temperatures: (a) 270 °C; (b) 280 °C; (c) 290 °C; (d) 300 °C.

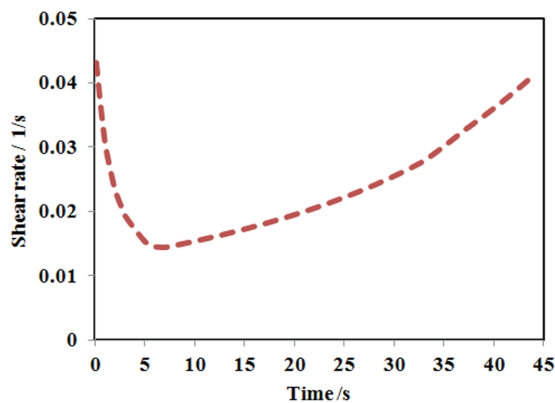


Figure 3. Simulated shear rate evolution near the center of upper disc at compressing speed 0.01 mm/s and melt temperature 290 °C

4.3 Compressing Speed Effects

To validate the modified PTT model determined by 0.01 mm/s compressing speed the other two experiments with compressing speeds of 0.005 and 0.02 mm/s were carried out at melt temperatures of 300 °C. The measured com-

pressing forces for these two speeds exhibited unstable growth especially at start stage for low speed and middle stage for high speed which can be hardly simulated by any constitutive model, see Fig. 4. So the simulated compressing force profiles are less precise than that of the same temperature with compressing speed 0.01 mm/s shown as Fig. 2 (d).

The simulated precisions of the two models for the three speeds were listed in Tab. 3. Once again Tab. 3 shows the modified PTT model is superior to the original model for any compressing speed as shear rate derivative $\dot{\gamma}$ was accounted in this model. Both average simulated differences and variances increase with increasing compression speeds either with PTT model or modified PTT model. When the compressing speed increases from 0.005 mm/s to 0.01 mm/s the average differences to experimental data for both models increase very little, but the variances rise about 3 and 2 times respectively. When the compressing speed continually increases to 0.02 mm/s the average simulated differences increase about 2 times of 0.005 mm/s, and the variances rise to about 21 and 10

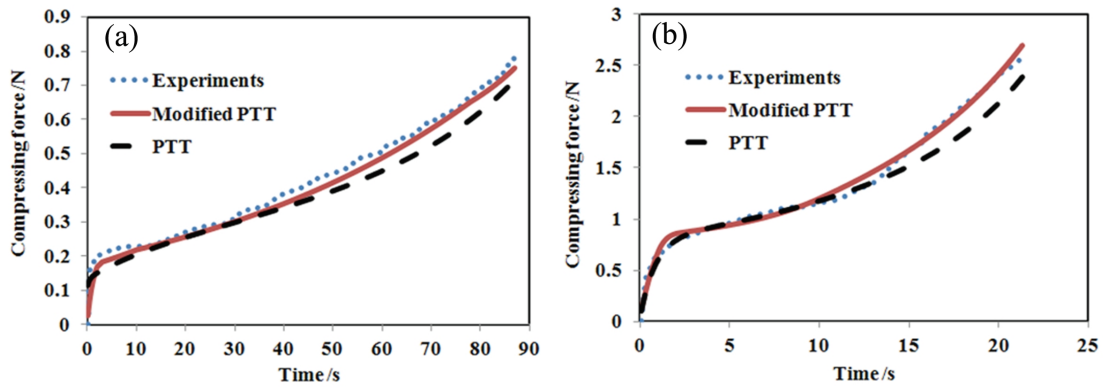


Figure 4. Compressing force varies with time for PC at melt temperature 300 °C with compressing speeds (a) 0.005 mm/s; (b) 0.02 mm/s

Table 3. Simulated precisions of the two models for the compressing speeds at temperature 300 °C

Compressing speed (mm/s)	PTT				Modified PTT			
	Difference			Variance	Difference			Variance
	Average	Start	End		Average	Start	End	
0.005	0.042634	0.045307	0.06339	0.000455	0.02059	0.027009	0.017221	0.000105
0.01	0.043427	0.022662	0.11008	0.001444	0.02439	0.013815	0.019223	0.000222
0.02	0.090167	0.079778	0.24856	0.009774	0.04460	0.063314	0.03559	0.001004

times of the low speed respectively. Because the measured data gets increasingly unstable as compressing speed increases, the simulated difference grows with the speed. Thus increasing the compressing speed can not get the credible data.

5. Conclusion

As the poor ability of the conventional constitutive models in describing the rheological behaviors in compressing start and end stages, the new viscoelastic model was proposed to overcome the shortage in this study. The shear rate derivative was added in the right side of PTT constitutive model to calculate the additional stresses induced by shear rate changes. The experimental results showed the modification improved simulating precisions especially for the compressing start and end stages. This study indicates the shear rate changes should be considered in constructing constitutive equations for unsteady flow. In addition, the flow becomes more unsteady when the compressing speed increases, which also makes the simulated differences increase.

Reference

[1] A.I. Isayev and R.K. Upadhyay, Injection and Compression Molding Fundamentals, Marcel Dekker, New York, 1987.
 [2] W. Cao, T. Wang, Y. Yan, et al. Evaluation of typical rhe-

ological models fitting for polycarbonate squeeze flow. J. Applied Polymer Sci. 2015, 132(29): 42279(1-8).
 [3] N. Phan-Thien, and R.I. Tanner, An analytical solution for fully developed from network theory, J. Non-Newtonian Fluid Mech. 1977, 2: 353-365.
 [4] N. Phan-Thien, A non-linear network viscoelastic model, J. Rheo. 1978, 22(3): 259-283.
 [5] B. Debbaut, Non-isothermal and viscoelastic effects in the squeeze flow between infinite plates, J. Non-Newtonian Fluid Mech. 2001, 98(1): 15-31.
 [6] J. D. Sherwood, Model-free inversion of squeeze-flow rheometer data, J. Non-Newtonian Fluid Mech. 2005, 129(2): 61-65.
 [7] J. H. Kim and K. Hyun, A new instrument for dynamic helical squeeze flow which superposes oscillatory shear and oscillatory squeeze flow, Rev. Sci. Instrum. 2012, 83(8): 085105(1-8).
 [8] D. Cheneler, J. Bowen, M.C.L. Ward, M.J. Adams, Micro squeeze flow rheometer for high frequency analysis of nano-litre volumes of viscoelastic fluid, Microelectronic Engineering 2011, 88(8): 1726-1729.
 [9] D. Cheneler, The Design and Analysis of a Micro Squeeze Flow Rheometer, Ph.D. Thesis, Department of Mechanical Engineering, University of Birmingham, UK, 2010.
 [10] R. G. Larson, A critical comparison of constitutive equations for polymer melts, J. Non-Newtonian Fluid Mech. 1987, 23(87): 249-268.

- [11] M. Aboubacar, H. Matallah, M.F. Webster, Highly elastic solutions for Oldroyd-B and Phan-Thien/Tanner fluids with a finite volume/element method: planar contraction flows, *J. Non-Newtonian Fluid Mech.* 2002, 103(1): 65–103.
- [12] A.S. Palmer and T.N. Phillips, Numerical approximation of the spectra of Phan-Thien Tanner liquids, *Numerical Algorithms* 2005, 38(1-3): 133-153.
- [13] W. Cao, C. Shen, C. Zhang et al, Computing flow-induced stresses of injection molding based on the Phan–Thien–Tanner model, *Archive of Applied Mechanics* 2008, 78(5): 363-377.
- [14] Y. Kobayashi, Y. Otsuki, H. Kanno, Y. Hanamoto, T. Kana, Crystallization of Polypropylene Near the Surface in Injection-Molded Plaques: A Comparison of Morphology and a Numerical Analysis, *POLYM. ENG. SCI.* 2011, 51(7): 1236–1244.
- [15] O. James, On the Formulation of Rheological Equations of State, *Proceedings of the Royal Society of London. Series A, Mathematical and Physical Sciences* 1950, 200: 523–541.
- [16] M. I. A. Othman, N. H. Sweilam, Electrohydrodynamic instability in a horizontal viscoelastic fluid layer in the presence of internal heat generation, *Can. J. Phys.* 2002, 80(6): 697–705.
- [17] M. I. A. Othman, Electrohydrodynamic stability in a horizontal viscoelastic fluid layer in the presence of a vertical temperature gradient, *Int. J. Eng. Sci.* 2001, 39(11): 1217-1232.
- [18] M. I. A. Othman, M. A. Ezzat, Electromagneto-hydrodynamic instability in a horizontal viscoelastic fluid layer with one relaxation time, *Acta Mechanica* 2001, 150(1-2): 1-9.
- [19] J. N. Sharma, R. Chand, M I. A. Othman, On the propagation of Lamb waves in viscothermoelastic plates under fluid loadings, *Int. J. Eng. Sci.* 2009, 47(3): 391-404.